Chapter 10
Integrated Submm Wave Receiver: Development and Applications

Valery P. Koshelets, Manfred Birk, Dick Boersma, Johannes Dercksen, Pavel Dmitriev, Andrey B. Ermakov, Lyudmila V. Filippenko, Hans Golstein, Ruud W.M. Hoogeveen, Leo de Jong, Andrey V. Khudchenko, Nickolay V. Kinev, Oleg S. Kiselev, Pavel V. Kudryashov, Bart van Kuik, Arno de Lange, Gert de Lange, Irina L. Lapitsky, Sergey I. Pripolzin, Joris van Rantwijk, Avri M. Selig, Alexander S. Sobolev, Mikhail Yu Torgashin, Vladimir L. Vaks, Ed de Vries, Georg Wagner, and Pavel A. Yagoubov

Abstract A superconducting integrated receiver (SIR) comprises in a single chip a planar antenna combined with a superconductor-insulator-superconductor (SIS) mixer, a superconducting Flux Flow Oscillator (FFO) acting as a Local Oscillator (LO) and a second SIS harmonic mixer (HM) for the FFO phase locking. In

V.P. Koshelets (✉) · A.B. Ermakov · A.V. Khudchenko · N.V. Kinev · O.S. Kiselev
Kotel'nikov Institute of Radio Engineering and Electronics, Russian Academy of Science, Mokhovaya st. 11/7, 125009, Moscow, Russia
and
SRON Netherlands Institute for Space Research, 9700 AV, Groningen, The Netherlands
e-mail: valery@hitech.cplire.ru; Khudchenko@hitech.cplire.ru

P. Dmitriev · P.V. Kudryashov · A.S. Sobolev · M. Yu Torgashin
Kotel'nikov Institute of Radio Engineering and Electronics, Russian Academy of Science, Mokhovaya st. 11/7, 125009, Moscow, Russia

D. Boersma · J. Dercksen · L.V. Filippenko · H. Golstein · R.W.M. Hoogeveen · L. de Jong · B. van Kuik · A. de Lange · G. de Lange · I.L. Lapitsky · J. van Rantwijk · A.M. Selig · Ed de Vries
SRON Netherlands Institute for Space Research, 9700 AV, Groningen, The Netherlands

M. Birk · G. Wagner
DLR German Aerospace Centre, Remote Sensing Technology Institute, 82234, Wessling, Germany

S.I. Pripolzin · V.L. Vaks
Institute for Physics of Microstructure, Russian Academy of Science, Ulyanova 46, GSP-105, Nizhny Novgorod, Russia

P.A. Yagoubov
SRON Netherlands Institute for Space Research, 9700 AV, Groningen, The Netherlands
and
European Organization for Astronomical Research in the Southern Hemisphere (ESO), Karl-Schwarzschild-Strasse 2, 85748, Garching bei München, Germany

this report, an overview of the SIR and FFO developments and optimizations is presented. Improving on the fully Nb-based SIR we have developed and studied Nb–AlN–NbN circuits, which exhibit an extended operation frequency range. Continuous tuning of the phase locked frequency has been experimentally demonstrated at any frequency in the range 350–750 GHz. The FFO free-running linewidth has been measured between 1 and 5 MHz, which allows to phase lock up to 97% of the emitted FFO power. The output power of the FFO is sufficient to pump the matched SIS mixer. Therefore, it is concluded that the Nb–AlN–NbN FFOs are mature enough for practical applications.

These achievements enabled the development of a 480–650 GHz integrated receiver for the atmospheric-research instrument TErahertz and submillimeter LImb Sounder (TELIS). This balloon-borne instrument is a three-channel superconducting heterodyne spectrometer for the detection of spectral emission lines of stratospheric trace gases that have their rotational transitions at THz frequencies. One of the channels is based on the SIR technology. We demonstrate for the first time the capabilities of the SIR technology for heterodyne spectroscopy in general, and atmospheric limb sounding in particular. We also show that the application of SIR technology is not limited to laboratory environments, but that it is well suited for remote operation under harsh environmental conditions. Light weight and low power consumption combined with broadband operation and nearly quantum limited sensitivity make the SIR a perfect candidate for future airborne and space-borne missions. The noise temperature of the SIR was measured to be as low as 120 K in double sideband operation, with an intermediate frequency band of 4–8 GHz. The spectral resolution is well below 1 MHz, confirmed by our measurements. Remote control of the SIR under flight conditions has been demonstrated in a successful balloon flight in Kiruna, Sweden.

Capability of the SIR for high-resolution spectroscopy has been successfully proven also in a laboratory environment by gas cell measurements. The possibility to use SIR devices for the medical analysis of exhaled air will be discussed. Many medically relevant gases have spectral lines in the sub-terahertz range and can be detected by an SIR-based spectrometer. The SIR can be considered as an operational device, ready for many applications.

10.1 Introduction

A Superconducting Integrated Receiver (SIR) [1, 2] was proposed more than 10 years ago and has since then been developed up to the point of practical applications [3–5]. Our approach consists in developing a *single chip* heterodyne receiver, which is smaller and less complex than traditional devices. Typically, such a receiver consists of a number of main components (local oscillator (LO), mixer, antenna structure, phase lock circuit, etc.), which are usually built as separate units and are complex (and thus costly). According to our concept (see Fig. 10.1), we have integrated all these components onto one single chip reducing overall system complexity in change for increased on-chip and lithographic fabrication complexity.
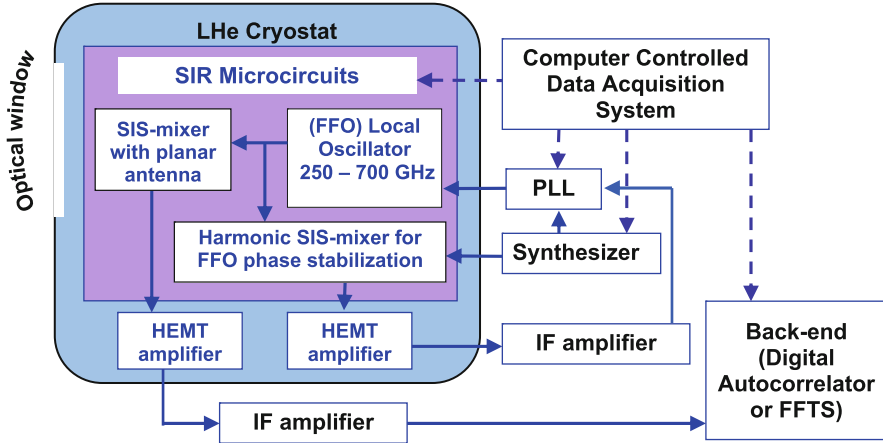
Fig. 10.1 Block-diagram of the superconducting integrated receiver

An SIR comprises on one chip all key elements needed for heterodyne detection: a low-noise superconductor-insulator-superconductor (SIS) mixer with quasi-optical antenna, a flux-flow oscillator (FFO) [6] acting as an LO and a second SIS harmonic mixer (HM) for the FFO phase locking. The concept of the SIR is very attractive for many practical applications because of the compactness and the wide tuning range of the FFO [7]. Presently, the frequency range of most practical heterodyne receivers is limited by the tuning range of the LO, typically 10%–15% for a solid-state multiplier chain [8]. In the SIR, the bandwidth is determined by the SIS mixer tuning structure and the matching circuitry between the SIS and the FFO. A bandwidth up to 30%–40% may be achieved with a twin-junction SIS mixer design. Another potential advantage is the use of arrays of SIR channels within a single cryostat that could operate at the same or different LO frequencies.

One of the important practical application of the SIR is TErahertz and sub-millimeter LImb Sounder (TELIS) [5, 9, 10] – a three-channel balloon-borne heterodyne spectrometer for atmospheric research developed in a collaboration of four institutes: Deutsches Zentrum für Luft- und Raumfahrt (DLR), Germany, Rutherford Appleton Laboratories (RAL), United Kingdom, and SRON – Nether-lands Institute for Space Research, the Netherlands (in tight collaboration with Kotel'nikov Institute of Radio Engineering and Electronics, IREE, Moscow). All three receivers utilize state-of-the-art superconducting heterodyne technology and operate at 500 GHz (by RAL), at 480–650 GHz (by SRON + IREE), and at 1.8 THz (by DLR). TELIS is a compact, lightweight instrument capable of providing broad spectral coverage, high spectral resolution and long flight duration. The TELIS instrument serves also as a test bed for many novel cryogenic technologies and as a pathfinder for satellite-based instrumentation.

TELIS is mounted on the same balloon platform as the Fourier transform spectrometer MIPAS-B [11], developed by IMK (Institute of Meteorology and

Climate research of the University of Karlsruhe, Germany) and is operated in the mid-infrared (680–2,400 cm^{-1}). Both instruments observe simultaneously the same air mass, and together they yield an extensive set of stratospheric constituents that can be used for detailed analysis of atmospheric chemical models, such as ozone destruction cycles. In particular, the 480–650 GHz TELIS channel is able to measure vertical profiles of ClO, BrO, O_3 and its rare isotopologues, O_2, HCl, HOCl, H_2O and three rare isotopologues, HO_2, NO, N_2O, NO_2, HNO_3, CH_3Cl, and HCN. In this paper, the design and technology for the 480–650 GHz channel as used in the flight configuration are presented in conjunction with test results and the first preliminary scientific results.

10.2 Flux Flow Oscillators

A Josephson Flux Flow Oscillator (FFO) [6] has proven [4, 5, 7] to be the most developed superconducting LO for integration with an SIS mixer in a single-chip submm-wave SIR [1–5]. The FFO is a long Josephson tunnel junction of the overlap geometry (see Fig. 10.2) in which an applied dc magnetic field and a dc bias current, I_B, drive a unidirectional flow of fluxons, each containing one magnetic flux quantum, $\Phi_0 = h/2e \approx 2 \times 10^{-15}$ Wb. Symbol h is Planck's constant and e is the elementary charge. An integrated control line with current I_{CL} is used to generate the dc magnetic field applied to the FFO. According to the Josephson relation, the junction oscillates with a frequency $f = (1/\Phi_0)V$ (about 483.6 GHz/mV) if it is biased at voltage V. The fluxons repel each other and form a chain that moves along the junction. The velocity and density of the fluxon chain and thus the power and frequency of the submm-wave signal emitted from the exit end of the junction due to the collision with the boundary may be adjusted independently by proper settings of I_B and I_{CL}. The FFO differs from the other members of the Josephson oscillator family by the need for these two control currents, which in turn provides the possibility of independent frequency and power tuning.

We experimentally investigated a large number of the FFO designs. The length, L, and the width, W, of the FFO used in our study are 300–400 μm and 4–28 μm,
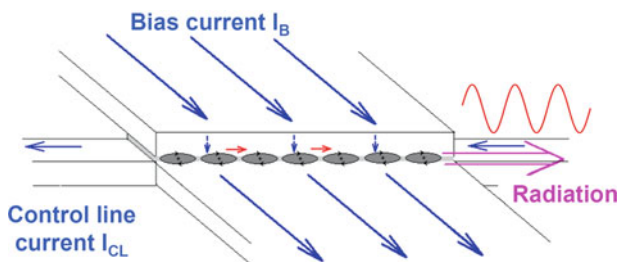
**Fig. 10.2** Schematic view of a flux-flow oscillator

respectively. The value of the critical current density, J_C, is in the range 4–8 kA/cm^2 giving a Josephson penetration depth, $\lambda_J \sim$ 6–4 μm. The corresponding value of the specific resistance is $Rn \times L \times W$ *is* $\sim$ 50–25 Ω μm^2. For the numerical calculations, we use a typical value of the London penetration depth, $\lambda_L \approx$ 90 nm for all-Nb junctions, and a junction specific capacitance, $Cs \approx 0.08$ pF/μm^2. The active area of the FFO (i.e. the AlO$_x$ or the AlN tunnel barrier) is usually formed as a long window in the relatively thick (200–250 nm) SiO$_2$ insulation layer sandwiched between the two superconducting films (base and wiring electrodes). The so-called "idle" region consists of the thick SiO$_2$ layer adjacent to the junction (on both sides of the tunnel region) between the overlapping electrodes. It forms a transmission line parallel to the FFO (not shown in Fig. 10.2). The width of the idle region ($W_I =$ 2–14 μm) is comparable to the junction width. The idle region must be taken into account when designing an FFO with the desired properties. In our design, it is practical to use the flat bottom electrode of the FFO as a control line in which the current I_{CL} produces the magnetic field, which mainly is applied perpendicular to the long side of the junction.

There are a number of important requirements on the FFO properties to make it suitable for application in the phase locked SIR. Obviously, the FFO should emit enough power to pump an SIS mixer, taking into account a specially designed mismatch of about 5–7 dB between the FFO and the SIS mixer, introduced to avoid leakage of the input signal to the LO path. It is a challenge to realize the ultimate performance of the separate superconducting elements after their integration in a single-chip device. Implementation of the improved matching circuits and the submicron junctions for both the SIS and the HM allows delivering optimal FFO power for their operation.

Even for ultra wideband room-temperature PLL systems the effective regulation bandwidth is limited by the length of the cables in the loop (about 10 MHz for typical loop length of two meters). It means that the free-running FFO linewidth (LW) has to be well below 10 MHz to ensure stable FFO phase locking with a reasonably good spectral ratio (SR) – the ratio between the carrier and total power emitted by the FFO [7]. For example, only about 50% of the FFO power can be phase locked by the present PLL system at a free-running FFO LW of 5 MHz. A low spectral ratio results in a considerable error at resolving the complicated spectral line shape [12]. Thus, a sufficiently small free-running FFO LW is vitally important for the realization of the phase locked SIR for the TELIS.

10.2.1 **Nb–AlN–NbN** *FFO*

Earlier the Nb–AlOx–Nb or Nb–AlN–Nb trilayers were successfully used for the FFO fabrication. Traditional all-Nb circuits are being constantly optimized but there seems to be a limit for LW optimizations at certain boundary frequencies due to Josephson self-coupling (JSC) effect [13] as well as a high frequency limit, imposed by Nb gap frequency ($\sim$700 GHz). That is the reason for novel types
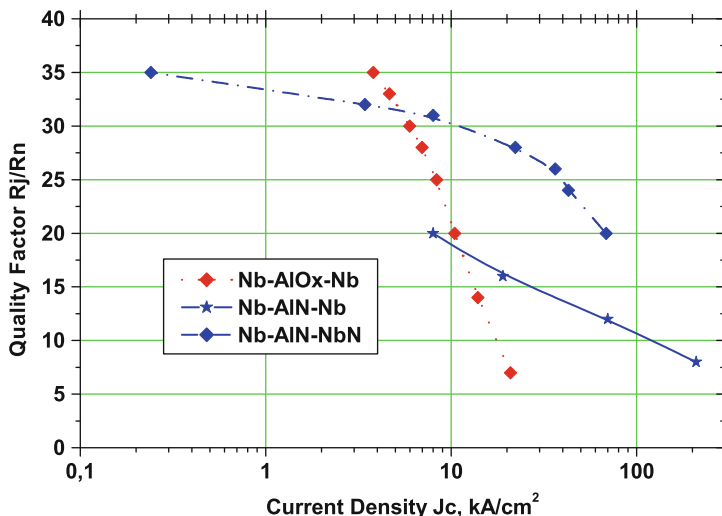
Fig. 10.3 The dependencies of Rj/Rn ratio on critical current density J_c for SIS junctions of different types fabricated at IREE

of junctions based on materials other than Nb to be developed. We reported on development of the high quality Nb–AlN–NbN junction production technology [14]. The implementation of an AlN tunnel barrier in combination with an NbN top superconducting electrode provides a significant improvement in SIS junction quality. The gap voltage of the junction $V_g = 3.7$ mV. From this value, and the gap voltage of the Nb film $\Delta_{Nb}/e = 1.4$ mV, we have estimated the gap voltage of our NbN film as $\Delta_{NbN}/e = 2.3$ mV [15].

The dependency of the ratio of subgap to normal state resistance (Rj/Rn) vs. critical current density (J_c) for different types of the Nb-based junctions fabricated at IREE is presented in Fig. 10.3. One can see that the Nb–AlN–NbN junctions are of very good quality at high current densities, important for implementation in THz mixers. The same technique was further used to produce complicated integrated circuits comprising SIS and FFO in one chip.

The use of Nb for top "wiring" layer is preferable due to lower losses of Nb compared to NbN below 720 GHz; furthermore, the matching structures developed for the all-Nb SIRs can be used directly for the fabrication of receivers with Nb–AlN–NbN junctions. The general behavior of the new devices is similar to the all-Nb ones; even the control currents, necessary to provide magnetic bias for FFO, were nearly the same for the FFOs of similar design.

A family of the Nb–AlN–NbN FFO IVCs measured at different magnetic fields produced by the integrated control line is presented in Fig. 10.4 ($L = 300\,\mu$m, $W = 14\,\mu$m, $W_I = 10\,\mu$m). A single SIS junction with an inductive tuning circuit is employed as a HM for the LW measurements. The tuning and matching circuits were designed to provide "uniform" coupling in the frequency range 400–700 GHz.
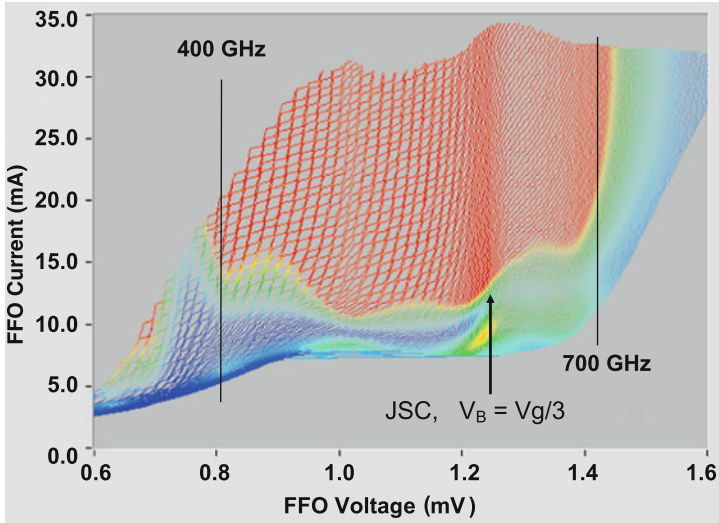
Fig. 10.4 IVCs of the Nb–AlN–NbN FFO measured at different magnetic fields produced by the integrated control line. The *color scale* shows the level of the DC current rise at the HM induced by the FFO. *Red area* marks the region of the FFO parameters where the induced by FFO HM current exceeds 25% of the I_g. This level is well above the optimal value for an SIS-mixer operation

Measured values of the HM current induced by the FFO oscillations (HM pumping) are shown in Fig. 10.4 by the color scale. The HM pumping for each FFO bias point was measured at constant HM bias voltage of 3 mV (pumping is normalized on the current jump at the gap voltage, $I_g = 140\,\mu A$). From Fig. 10.4, one can see that an FFO can provide large enough power over the wide frequency range: limited at higher frequencies only by the Nb superconducting gap in transmission line electrodes (base and wiring layers) and below 400 GHz by design of the matching circuits.

The Nb–AlN–NbN FFOs behave very similar to all-Nb ones. The feature at about 600 GHz where the curves get denser is a Josephson Self-Coupling (JSC) boundary voltage. It was first observed for all-Nb FFOs [13]. The JSC effect is the absorption of the FFO-emitted radiation by the quasi-particles in the cavity of the long junction. It considerably modifies the FFO properties at the voltages $V \approx V_{JSC} = 1/3V_g$ (V_{JSC} corresponds to 620 GHz for the Nb–AlN–NbN FFO). Just above this voltage, the differential resistance increases considerably; that results in an FFO-LW broadening just above this point. This, in turn, makes it difficult or impossible to phase lock the FFO in that region. For a Nb–AlOx–Nb FFO, the transition corresponding *to $V_{JSC} = V_g/3$* occurs around 450 GHz. So, by using the Nb–AlN–NbN FFOs we can cover the frequency gap from 450 to 550 GHz imposed by the gap value of all-Nb junctions. The feature in Fig. 10.4 around 1 mV is very likely due to a singularity at the difference of the superconducting gaps $\Delta_{NbN} - \Delta_{Nb}$.

Continuous frequency tuning at frequencies below 600 GHz for the Nb−AlN−NbN FFOs of moderate length is possible, although the damping is not sufficient to completely suppress the Fiske resonant structure at frequencies below $V_g/3$. For short junctions with a small α (wave attenuation factor), the distance between the steps in this resonant regime can be as large, that it is only possible to tune the FFO at the certain set of frequencies. For a 300–400 μm long Nb–AlN–NbN junction, this is not the case – the quality factor of the resonator formed by a long Nb–AlN–NbN Josephson junction is not so high at frequencies >350 GHz. Therefore, the resonance steps are slanting and the distance between them is not so big (see Fig. 10.4). This allows us to set any voltage (and any frequency) below V_{JSC}, but for each voltage only a certain set of currents should be used. So, in this case we have the regions of forbidden bias-current values, specific for each voltage below V_{JSC}, instead of the forbidden voltage regions for the Fiske regime in Nb–AlOx–Nb FFO [15]. Special algorithms have been developed for automatic working point selection in flight.

In Fig. 10.5, the typical current-voltage characteristics (IVCs) of a Nb–AlN–NbN SIS junction of an area of about 1 μm² is given, both the unpumped IVC (solid line) and the IVC when pumped by a Nb–AlN–NbN FFO at different frequencies (dotted lines). One can see that the FFO provides more than enough power for the mixer pumping. In this experiment, we use the test circuits with low-loss matching circuits tuned between 400 and 700 GHz. Even with the specially introduced 5 dB FFO/SIS mismatch (required for the SIR operation) the FFO delivers enough power for the SIS mixer operation in the TELIS frequency range of 480–650 GHz [7].
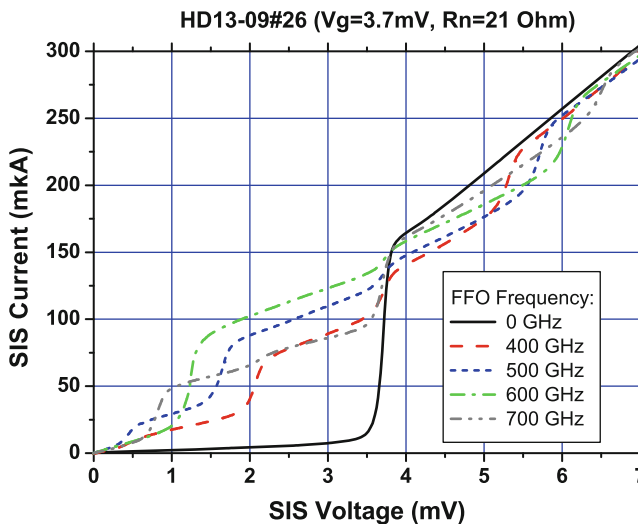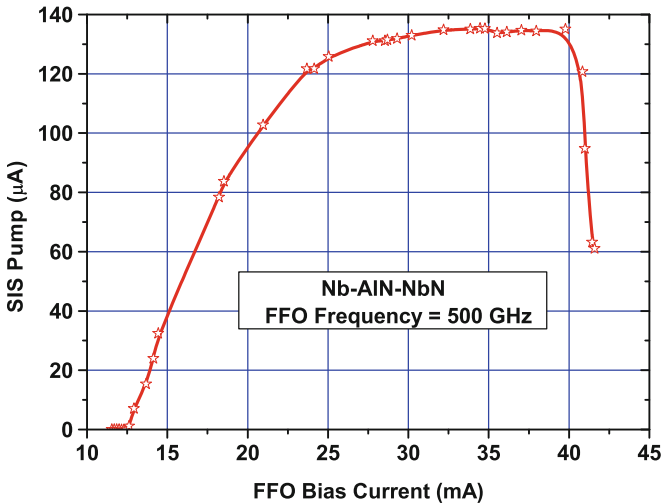

Fig. 10.5 The IVCs of the SIS mixer: unpumped – *solid curve*, pumped at different frequencies – *dashed and dotted lines*
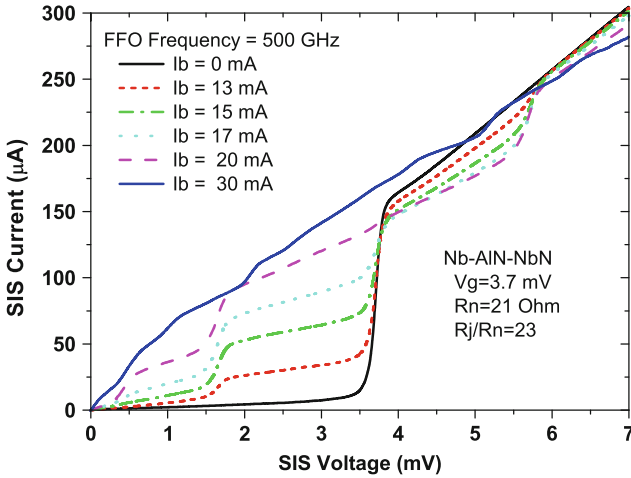
Fig. 10.6 The IVCs of the SIS mixer: unpumped – *black solid curve*, pumped at different FFO bias currents (different powers) – lines with symbols; FFO frequency = 500 GHz

Fig. 10.7 The pump current of the SIS mixer biased at 3 mV as a function of the FFO bias current at the fixed frequency 500 GHz (see Figs. 10.4 and 10.6)

An important issue for the SIR operation is a possibility to tune the FFO power, while keeping the FFO frequency constant. This is demonstrated in Fig. 10.6, where the IVCs of an SIS mixer are shown, while being pumped at different FFO bias currents (different powers). The dependence of the SIS pump current on the FFO bias current is presented in Fig. 10.7, showing that the FFO power can be tuned more than 15 dB, while keeping the same frequency by proper adjustment of the control line current.

10.2.2 Spectral Properties of the FFO

10.2.2.1 LW Measurements

The FFO LW has been measured in a wide frequency range from 300 GHz up to 750 GHz using a well-developed experimental technique [16]. A specially designed integrated circuit incorporates the FFO junction, the SIS HM and the microwave matching circuits. Generally, both junctions are fabricated from the same Nb/AlN/NbN or Nb/AlOx/Nb trilayer. The FFO signal is fed to the SIS HM together with a 17–20 GHz reference signal from a stable synthesizer. The required power level depends on the parameters of the HM; it is about of $1\,\mu W$ for a typical junction area of $1\,\mu m^2$. The intermediate frequency (IF) mixer product ($f_{IF} = \pm(f_{FFO} - n \cdot f_{SYN})$ at ~ 400 MHz is first boosted by a cooled HEMT amplifier ($T_n \sim 5$ K, gain $= 30$ dB) and then by a high-gain room-temperature amplifier.

To accurately measure the FFO line shape, the IF signal must be time-averaged by the spectrum analyzer. To remove low-frequency drift and interference from the bias supplies, temperature drift, etc., we use a narrow bandwidth (<10 kHz) Frequency Discriminator (FD) system with relatively low loop gain for *frequency locking* of the FFO. With the FD narrow-band feedback system that stabilizes the mean frequency of the FFO (but does not affect FFO line shape), we can accurately measure the free-running FFO LW, which is determined by the much faster internal ("natural") fluctuations (see Fig. 10.8).
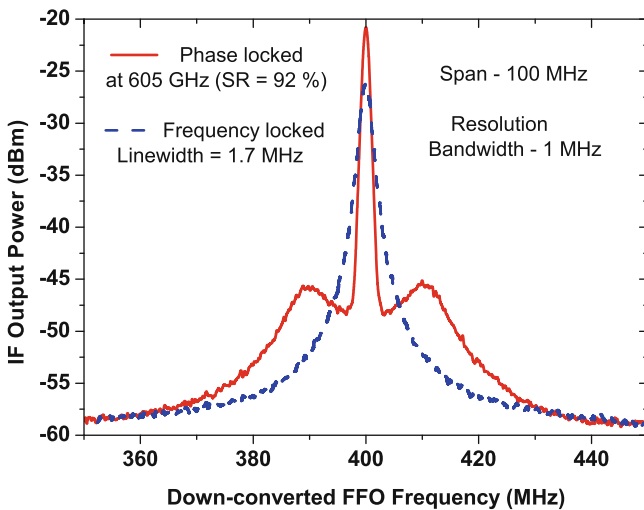
Fig. 10.8 Spectra of the Nb–AlN–NbN FFO operating at 515.2605 GHz (*blue dashed line* – frequency locked by FD; *red solid line* – phase-locked). Linewidth $= 1.7$ MHz; spectral ratio $= 92\%$

The resulting IF signal is supplied also to the Phase Locking Loop (PLL) system. The phase-difference signal of the PLL is fed to the FFO control line current. Wideband operation of the PLL (10–15 MHz full width) is obtained by minimizing the cable loop length. A part of the IF signal is delivered to the spectrum analyzer through a power splitter (see Fig. 10.8). All instruments are synchronized to harmonics of a common 10 MHz reference oscillator.

The integrated HM may operate in two different regimes, either as a quasi-particle mixer (SIS) or as a Josephson mixer. To exclude the noise from the Josephson super-current fluctuations and thereby realize a pure quasi-particle regime, the super current has to be suppressed by a relatively large magnetic field. This requires a special control line placed near the SIS mixer. The quasi-particle regime of the HM operation can also be realized with sufficient synthesizer power. It has been shown [17] that the FFO LW and signal-to-noise ratio are almost the same for these two regimes, although the phase noise might be somewhat lower in the quasi-particle mode.

10.2.2.2   Dependence of the FFO Linewidth on FFO' Parameters

Detailed measurements of the FFO LW [18, 19] demonstrate a Lorentzian shape of the free-running FFO line in a wide frequency range up to 750 GHz, both at higher voltages on the flux flow step (FFS) and at lower voltages in the resonant regime on the Fiske steps (FSs). This implies that the free-running ("natural") FFO LW in all operational regimes is determined by the wideband thermal fluctuations and the shot noise. This is different from many traditional microwave oscillators, where the "natural" LW is very small and the observed LW can be attributed mainly to external fluctuations. It was found [18, 19] that the free-running FFO LW, δf, exceeds theoretical estimations made for lumped tunnel Josephson junction. The expression for the LW dependency on voltage and differential resistances found for all-Nb FFOs [18, 20] is valid for Nb–AlN–NbN junctions as well:

$$\delta f = \left(2\pi/\Phi_0^2\right)\left(R_d^B + K * R_d^{CL}\right)^2 S_i(0), \qquad (10.1)$$

where S_i0 is the power density of low frequency current fluctuations, R_d^B and R_d^{CL} are differential resistances on bias and control line currents, respectively. Note that ratio R_d^{CL}/R_d^B is constant for fixed FFO bias, so $\delta f = A(I_B)(R_d^B)^2 S_i0$.

Earlier, a so-called Super Fine Resonance Structure (SFRS) [21] was observed on the FFO IVCs, resulting in the jumps of the FFO between tiny steps (frequency spacing is of about 10 MHz, see Fig. 10.9). The presence of the SFRS prohibits phase locking at frequencies between the steps. This is unacceptable for practical applications. Recently, we found that the SFRS is related to interference of the acoustic waves created by the FFO (generation of the phonons by Josephson junction, see [22]). A special technological procedure allows us to eliminate this interference and to realize continuous FFO-frequency tuning in the SIR, being
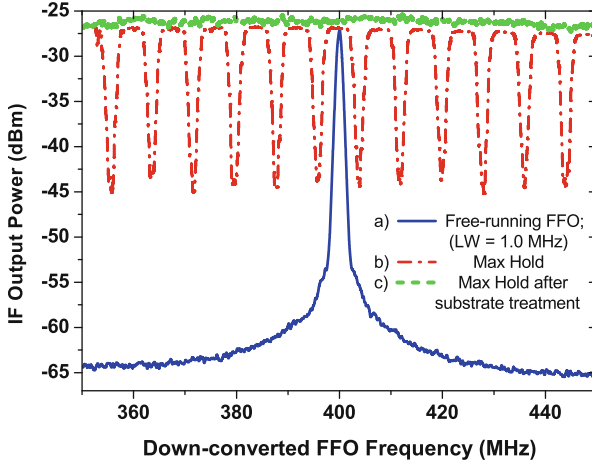
Fig. 10.9 Down-converted spectra of the FFO: (**a**) free-running FFO; (**b**), (**c**) – the lines show the maximum FFO signal level recorded in the MaxHold regime of the Spectrum Analyzer (the top point of curve "a") on the FFO frequency, measured before (**b**) and after (**c**) special Si substrate treatment
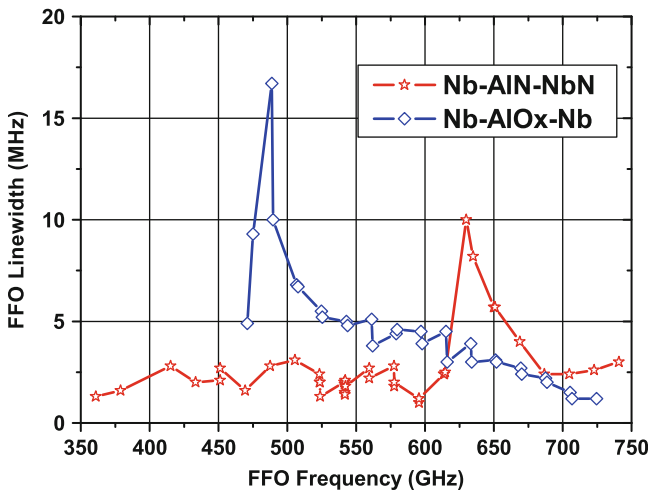

Fig. 10.10 Linewidth dependency on frequency for two types of the FFO

vitally important for TELIS project (see Fig. 10.9). Details of this study will be published elsewhere.

In Fig. 10.10, we present a comparative graph of the free-running FFO LW for two types of the tri-layer. One can see that the LW of Nb–AlN–NbN FFO is twice as small up to 600 GHz. It should be emphasized that due to overlapping FSs continuous tuning is possible and any desirable frequency can be realized. Several

"stacked" stars at certain frequencies for the NbN FFO mean that the best LW value
can be selected by adjusting FFO bias. Note that the spread in the LW values at
a selected frequency is small and all can actually be applied for measurements.
Each star corresponds to an "allowed" bias current at an FS (as described above in
Sect. 2.1). Although the FFO tuning on an FS is complicated, the benefit in LW (and
consequently the spectral ratio) is worth the effort. Linewidths below 3 MHz can
be achieved in the whole range between 350 and 610 GHz. An abrupt increase of
the FFO LW at some frequencies is caused by the Josephson self-coupling effect.
The JSC (absorption of the FFO-emitted radiation by the quasi-particles in the
cavity of the long junction, see above) considerably modifies the FFO properties
at the voltages $V \approx V_{JSC} = 1/3 V_g$ [13] (V_{JSC} corresponds to 620 GHz for the
Nb–AlN–NbN FFO).

Previous LW measurements have demonstrated [7, 23] the essential dependences
of the free-running FFO LW on the FFO voltage, its current density and geometry
of the biasing electrodes. In this report, we summarize the results of the FFO study
and optimization of the FFO layout for both types of FFOs. Recently, it was shown
[4, 7] that the LW decreases considerably with increasing width, W, of the FFO
junction. This is valid for all frequencies of interest, and consequently, the spectral
ratio of the phase locked FFO for wide junctions is better. We have increased the
FFO width up to 28 μm, which is more than five times the Josephson penetration
depth λ_J. A number of FFOs with the same electrode layout, but different widths
of the FFO junction ($W = 4, 8, 12, 16, 20$ and 28 μm) are fabricated using the
same technological procedure yielding the same junction parameters (normal state
resistance × area, $RnS = 30\,\Omega\,\mu m^2$). The results of the LW measurements of these
circuits at three frequencies are presented in Fig. 10.11.
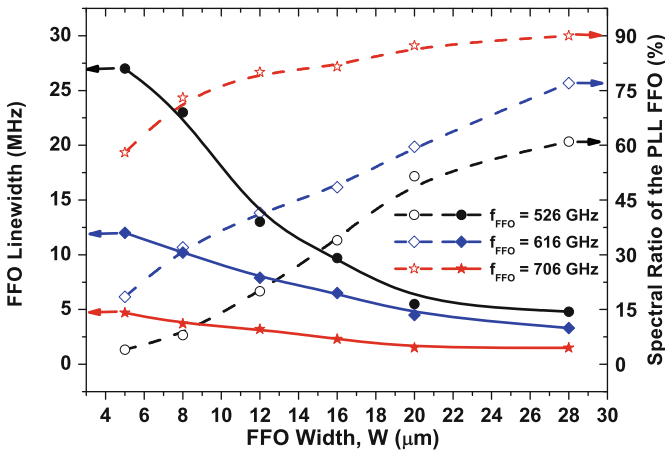
Fig. 10.11 Linewidth of free-running FFOs (*left axis*) and corresponding spectral ratio for the
phase-locked FFO (*right axis*) measured at different FFO frequencies as a function of FFO width.
All circuits are fabricated by the same technological procedure (RnS $= 30\,\Omega\,\mu m^2$)

Even for the largest tested width ($W = 28\,\mu\text{m}$), there is no evidence of deterioration in the FFO behaviour. Furthermore, the power delivered to the SIS mixer is getting higher and the LW lower at all frequencies. The decrease of the FFO LW with increasing FFO width is in accordance with existing theoretical models and our expectations. The bias current differential resistance, R_d, decreases approximately inversely proportional to the bias current I_B. Since the FFO LW is proportional to $R_\text{d}^{2*}I_\text{B}$, it scales down linearly with the junction width. Of course, one can expect that the LW decrease will saturate and the FFO performance will deteriorate with further increase of the width (e.g., due to appearance of transversal modes). Without a reliable theory, the optimal value of the FFO width has to be determined experimentally. Note that for a wider FFO the center line of the junction is shifted away from the edge of the control line (the R_d^{CL} goes down). This may result in a considerable reduction of extraneous noise from external magnetic fields. Furthermore, a wider FFO presumably will have a more uniform bias current distribution [4]. At the present state, the width of the FFO for TELIS is chosen to be $16\,\mu\text{m}$. This is a tradeoff between LW requirements and technical limitation on the maximum bias and control line currents (both should not exceed 70 mA).

In contrast to variation of the FFO LW on the FFO width, previous measurements [7] have demonstrated a considerable increase of the FFO LW with the FFO current density. This contradicts the simplified consideration: the increase of the FFO current density (as it is for increase of the FFO width) should result in the increase of the total FFO bias current, I_B, and reduce the FFO differential resistance on the bias current R_d. Since the FFO LW is proportional to $R_\text{d}^{2*}I_\text{b}$, one should expect the decrease of the measured FFO free-running LW for larger FFO current density. In reality, R_d does not decrease as much as this simple consideration predicts and the LW increases. On the contrary, a high value of the current density ($J_\text{c} \geq 8\,\text{kA/cm}^2$) is important for wide-band operation of the SIS-mixer at the submm wave range. The increase of the FFO LW with current density (as discussed above) creates a serious problem in the design and development of SIR chips. Implementation of two separate tri-layers with different current densities – one for the SIS mixer (high J_c) and the other one for the FFO/HM (lower J_c) seems to be a solution. We have successfully tested and verified this approach for the SIR microcircuits for TELIS.

Improvement of the FFO performance was obtained by enlarging the electrodes overlapping area, the so-called "idle region". Larger overlapping presumably provides a more uniform bias-current distribution, due to reduced inductance of the overlapping electrodes. Larger overlapping of the FFO electrodes also implies that the FFO of the same width is shifted from the edge of the bottom electrode, resulting in a considerable decrease of the R_d^{CL} value. Note that for a wide FFO also some shift of the FFO center line appears due to increasing of the width. Experimentally, we found that an idle region $W_\text{I} = 10\,\mu\text{m}$ is the optimal value for the present FFO design. Up to now, there is no adequate model that can quantitatively describe both the processes in the FFO and a self-consistent distribution of the bias current. Nevertheless, the presented results are very encouraging and these modifications of the FFO were implemented in the TELIS SIRs.

To further explore this approach, we have developed different designs of the "self-shielded" FFO with a large ground plane in the base electrode. Such FFOs are expected to be less sensitive for variations in the external magnetic field and have to provide more uniform bias current distribution (since all bias leads are laying over superconducting shield and have low inductance). Actually, the low-inductive bias leads provide a possibility of optimal (rather than uniform) current distribution, "regulated" by the FFO itself. The last feature optimizes the emitted FFO power. Indeed, the IVCs of all shielded FFOs are much more reproducible; the power delivered to HM is higher compared to a traditional design. Unfortunately, the free-running LW for all variants of shielded FFOs with separate bias leads is much larger than for FFOs of traditional design. It seems that injection of the bias via separate leads results in some spatial modulation of bias current [23] despite the additional triangular elements added for more uniform current injection. On the contrary, designs that employed three superconducting electrodes provide both perfect pumping and improved LW, details will be published elsewhere.

10.2.2.3   Spectral Ratio, Phase Noise

As it was mentioned above, the free-running FFO LW has to be well below 10 MHz to ensure stable FFO phase locking with a reasonably good spectral ratio (SR, the ratio between the carrier and total FFO power). For example, only about 50% of the FFO power can be phase locked by the present TELIS PLL system at free-running FFO LW of 5 MHz. A low spectral ratio results in a considerable error at resolving of the complicated atmospheric line shapes [12]. For the given PLL system, the value of the SR is fully determined by the free-running FFO LW: these two quantities are unambiguously related (see Fig. 10.12, where data for FFOs of different designs and types are presented). The theoretical curve, calculated in [24], coincides reasonably well with the experimental data. A possibility to considerably increase the SR by application of the ultra-wideband cryogenic PLL system has been recently demonstrated [25].

An important issue for TELIS operations is the possibility to tune the FFO frequency and power independently, while providing the same spectral ratio of PL FFO. The TELIS HM is pumped by a tunable reference frequency in the range of 19–21 GHz from the LO Source Unit (LSU), phase locked to the internal ultra stable 10 MHz Master Oscillator. The HM mixes the FFO signal with the n-th harmonic of the 19–21 GHz reference. The LW and SR of the TELIS FFO are almost constant over a wide range of FFO bias current at fixed FFO frequency (see Fig. 10.13). From this figure, one can see that the SR is about 50% over the range of bias current, I_b, 14–30 mA, while the pumping level varies from 3.5 µA at $I_b =$ 14 mA up to 81 µA at $I_b = 30$ mA. Furthermore, the SR $= 34\%$ can be realized at $I_b = 12$ mA, where the HM pumping is below 0.5 µA. It means that at proper choice of the HM voltage and LSU power even moderate HM pumping by the FFO is enough for efficient PLL operation (providing sufficient signal-to-noise ratio).
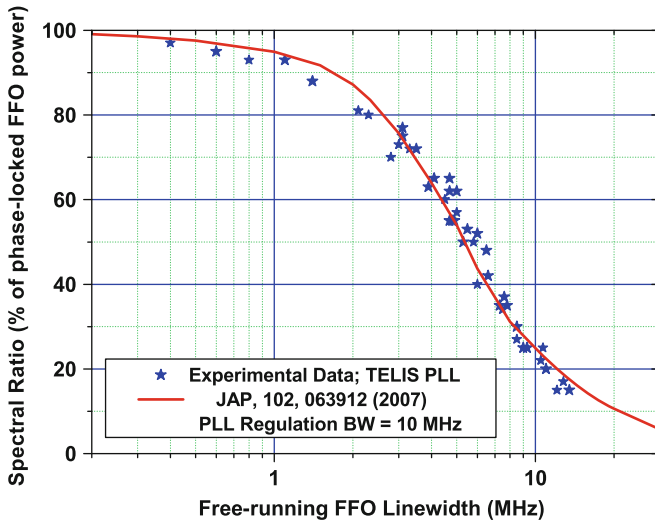
Fig. 10.12 Spectral ratio for the phase-locked FFO of different types and designs as a function of free-running FFO linewidth. *Solid line* – calculated dependence of the SR on FFO LW for PLL bandwidth $= 10\,\mathrm{MHz}$
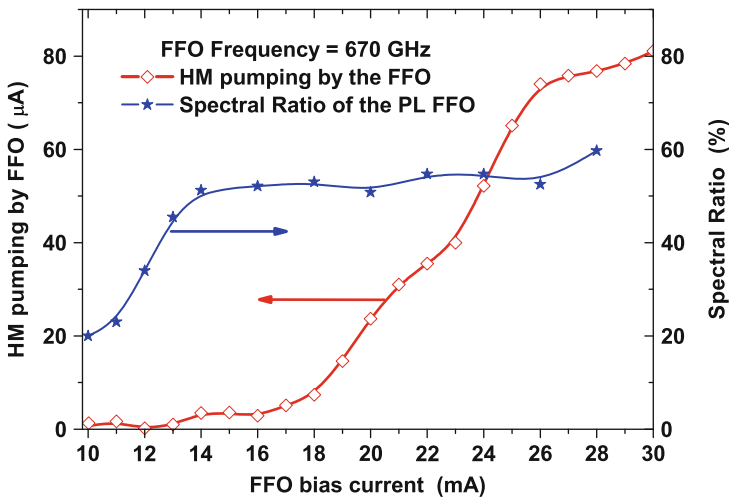
Fig. 10.13 Dependence of the HM current induced by FFO (HM pumping) and spectral ratio after FFO phase-locking as a function of FFO bias current. All the data measured at FFO frequency of 670 GHz

To prove the capabilities for high-resolution spectroscopy, line profiles around 625 GHz of OCS gas have been successfully measured by the SIR operating in the DSB regime [3]. The tests were done in a laboratory gas cell setup at a gas pressure down to 0.2 mBar, corresponding to the FWHM LW < 5 MHz. It was demonstrated

that the spectrum recorded by the Digital Auto Correlator (DAC) is a convolution product of the signal (gas emission lines) with the FFO line spectrum; resolution in this experiment is limited by DAC back-end. More detailed spectral measurements data will be presented in the next section.

To investigate the ultimate frequency resolution of the receiver, we have measured the signal of the synthesizer multiplied by a super-lattice structure [26]. The signal recorded in these measurements is a convolution of the narrow-bandwidth (delta-function-like) spectrum of the synthesizer with phase locked spectrum of the FFO with an accuracy of the used resolution bandwidth of the spectrum analyzer (30 kHz). It was confirmed that the frequency resolution of the receiver is better than 100 kHz.

The residual phase noise of the phase locked FFO – measured relative to the reference synthesizer – as a function of the offset from the carrier is plotted in Fig. 10.14. To get the absolute FFO phase noise, one should add the synthesizer noise multiplied by n^2 to the residual phase noise of the FFO. Data for the Rohde&Schwarz®SMF100A Microwave Signal Generator with improved phase noise [27] are also presented in Fig. 10.14, for the case where the FFO, operating at 450 GHz, is locked to the 20th harmonic of the synthesizer, $n^2 = 400$. The total (absolute) FFO phase noise (solid line in Fig. 10.14) is dominated by the synthesizer
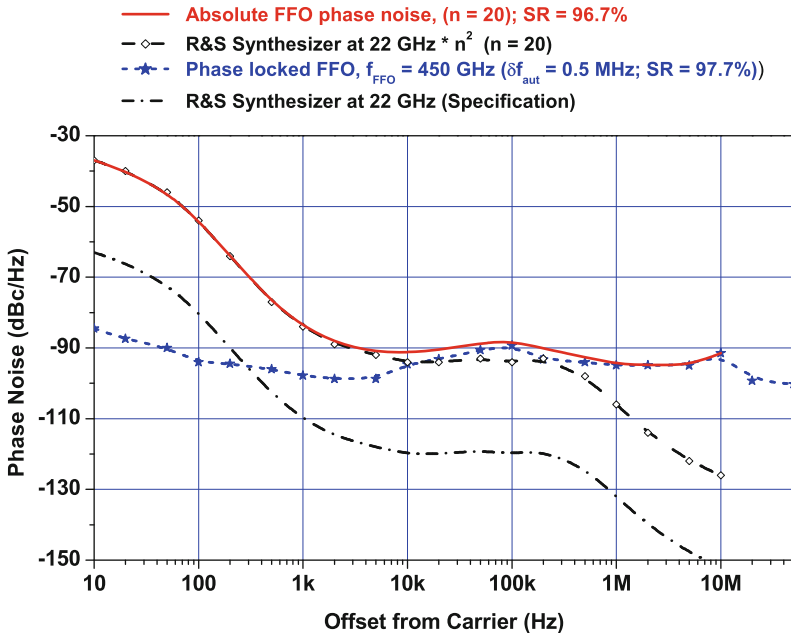
Fig. 10.14 Experimental phase noise of a phase locked FFO at 450 GHz. Since the phase noise of the FFO is measured relative to the 20th harmonic of the synthesizer, the synthesizer noise [27], multiplied by a factor $20^2 = 400$, should be added to the residual FFO noise to get the total (absolute) FFO phase noise – *solid line*

noise for offsets $< 10\,\text{kHz}$. The noise at larger frequency offset is mainly due to PLL system. Note that the FFO phase noise is overestimated since no subtraction of the noise added by the IF amplifier chain was performed; actually at offsets much larger than the PLL regulation bandwidth ($>20\,\text{MHz}$) the measured phase noise is mainly determined by the IF chain.

This section can be summarized as follows. Continuous tuning of the frequency is possible for Nb–AlN–NbN FFOs due to bending and overlapping of the FSs, so that any desirable frequency can be realized. A possibility to phase lock the Nb–AlN–NbN FFO at any frequency in the range 350–750 GHz has been experimentally demonstrated. An optimized design of the FFO for TELIS has been developed and tested. A free-running LW value from 5 to 1 MHz has been measured in the frequency range 300–750 GHz for a "wide" FFO. As a result, the spectral ratio of the phased locked FFO varies from 50% to 97% correspondingly. The "unlocked" rest of the total FFO power increases the phase noise and the calibration error. To ensure remote operation of the phase locked SIR several procedures for its automatic computer control have been developed and tested. New designs of the FFO intended for further improvement of its parameters are under development, but even at the present state the Nb–AlN–NbN FFOs are mature enough for practical applications.

10.3 TELIS

10.3.1 TELIS Instrument Design

The front-end of the ballon-borne TELIS instrument for atmospheric research is common for the three channels on board. It consists of the pointing telescope, a calibration blackbody, relay and band-separating optics (see Fig. 10.15). Details of
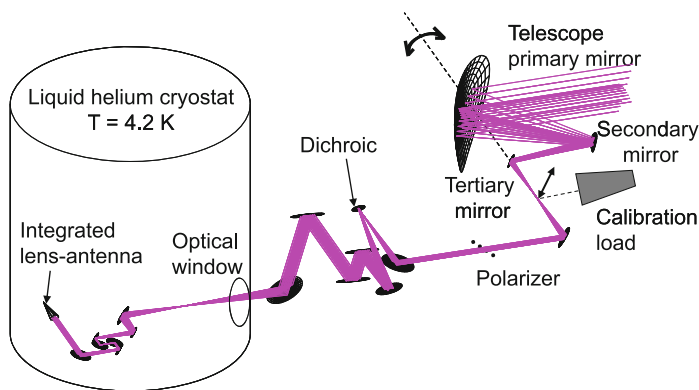
Fig. 10.15 Optical lay-out of the TELIS SIR channel

the optical design can be found in [28–30]. The three mirrors of the dual offset Cassegrain telescope are mounted on a common frame, rotatable around the optical axis of the output beam. Limb scanning is performed between the upper troposphere (8–10 km in the Arctic) to flight altitude (typically 32 km) in 1–2 km steps. At the tangent point of the line of sight, the vertical (elevation) resolution is about 2 km for an observational frequency of 500 GHz, scaling inversely proportional with frequency. In horizontal (azimuth) direction, the spatial resolution is about a factor of 2 less due to the anamorphicity of the telescope. This is allowed as the atmospheric properties within the beam hardly depend on the azimuth.

The radiometric gain of the spectrometers is calibrated once or twice in every Limb scan using a conical blackbody reference source and a measurement of the cold sky. For this, a small flip mirror is included between the telescope and the beam-separating optics. By measuring at two up-looking telescope positions, the impact of the remaining air above the gondola can be assessed.

Simultaneous observation by the receivers is achieved by quasi-optical beam splitting. First, a wire-grid-based polarizing beam splitter is employed to reflect one linear polarization to the 500 GHz channel, the other linear polarization is split by a dichroic filter between the SIR channel and the THz channel. Subsequently, offset mirrors shape and direct the three beams to the cryogenic channels. Inside the custom designed liquid-helium cooled cryostat, each receiver has dedicated cold optics, a superconducting mixing element and IF amplifiers.

The very compact 500 GHz receiver channel consists of a fixed-tuned waveguide SIS mixer, a cryogenic solid-state LO chain and a low-noise IF chain operating at a relatively high IF (IF = 15–19 GHz) [31]. The 1.8 THz channel employs a cryogenic solid-state LO that is loss-less coupled into the mixer via a Martin–Puplett type optical interferometer. The mixer is based on a phonon-cooled NbN HEB (Hot Electron Bolometer) [32]. The 480–650 GHz SIR receiver channel is based on a single-chip SIR, as described in the next section.

The warm optics couples to the SIR channel with a beam that has a waist radius ranging from 2 to 3 mm, located at the cryostat window. The system-pupil is imaged by two additional mirrors on the silicon elliptical lens; on the back surface of this lens, the SIR chip is located. The SIR-channel cold-optics is also frequency independent to fully exploit the wide-band operation of the SIR device.

The amplitude-phase distribution of the near field beam of the SIR cold channel at 600 GHz as measured at the dewar window is shown in Fig. 10.16. The beam waist is measured to be 2.25 mm, which is within 1% of the designed value. The measured Gaussisity of the beam is 92.4%.

The IF processor (located on the main frame of TELIS) converts the amplified IF output signals of the three receivers to the input frequency range of the digital autocorrelator. The digital autocorrelator has a bandwidth of 2×2 GHz with 2,048 spectral channels. Both the IF processor and the digital autocorrelator are developed by Omnisys Instruments AB [33].

The SIR channel is controlled with a battery-operated ultra low-noise biasing system. Since noise on the bias lines of the FFO translates in a wider FFO LW, several precautions, such as decoupling of digital control lines and extensive
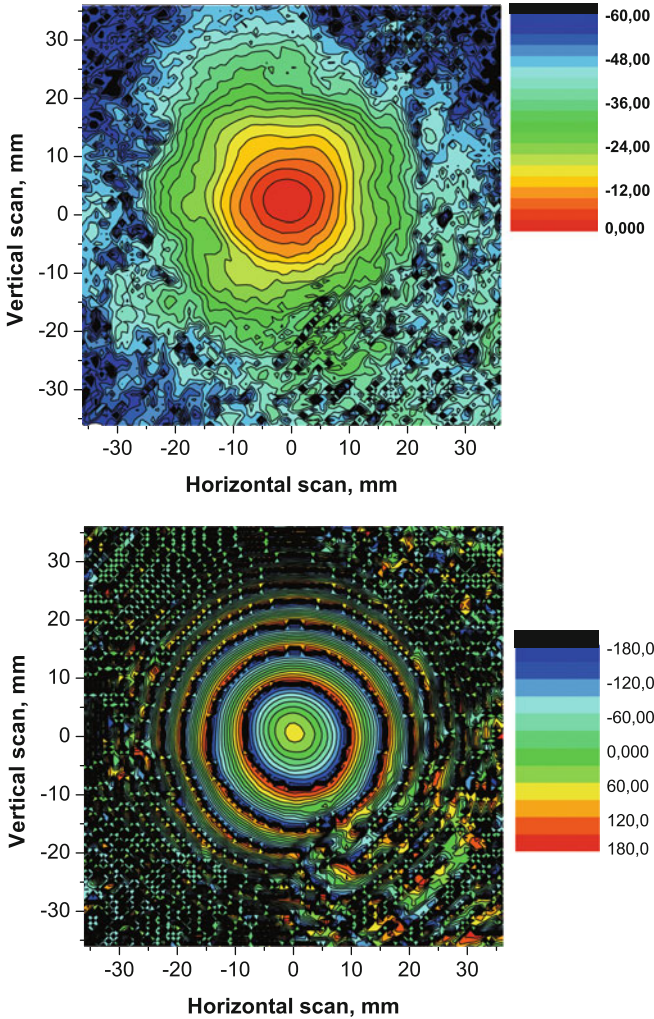
Fig. 10.16 The amplitude (*top figure*) and phase (*lower figure*) distribution of the near field beam of the SIR channel. The amplitude is given in units of dB. The distance from the beam waist is 110 mm and the frequency is 600 GHz

filtering and shielding, are implemented. The SIR bias unit is digitally controlled by the on-board DLR PC-104 computer, that also interfaces with the other channels, the digital autocorrelator, and with the host instrument MIPAS. A radio link provides real-time two-way contact with the ground segment consisting of a server computer with three dedicated client computers, coupled through TCP/IP socket connections. The complete system is dimensioned to have sufficient cooling liquids and battery power for a 24 h flight.
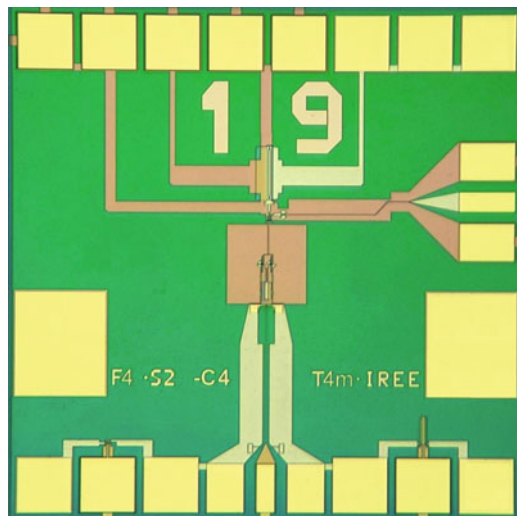
Fig. 10.17 Photo of the SIR microcircuit with double-slot antenna

10.3.2   SIR Channel Design

A key element of the 480–650 GHz channel is the SIR [1–5] that comprises in one chip (size of $4 \times 4 \times 0.5$ mm, see Fig. 10.17) a low-noise SIS mixer with quasioptical antenna, a superconducting FFO [6] acting as an LO and a second SIS HM for FFO phase locking. Since the free-running LW of the FFO can be up to 10 MHz, for spectral applications the FFO has to be locked to an external reference oscillator employing a phase lock loop(PLL) system. The concept of the SIR looks very attractive for TELIS due to a wide tuning range of the FFO. In the SIR, the bandwidth is basically determined by the SIS mixer tuning structure and matching circuitry between the SIS and FFO; bandwidth up to 30–40% may be achieved with a twin-junction SIS mixer design (both for double-slot and double-dipole antennas). To achieve the required instantaneous bandwidth of 480–650 GHz, a twin-SIS mixer with $0.8 \, \mu m^2$ junctions and new design of the FFO/SIS matching circuitry were implemented. A microscope photograph of the central part of the SIR chip with double-dipole antenna is presented in Fig. 10.18.

The resolution of the TELIS back-end spectrometer is 2.160 MHz, sufficient to resolve the exact shape of atmospheric lines. The FFO line shape and spectral stability should ideally be much better than this. However, the free-running LW of the FFO can be up to 10 MHz and therefore a PLL has been developed to phase lock the FFO to an external reference oscillator [6, 14]. For this, a small fraction of the FFO power is first directed to a so-called HM, placed on the SIR chip. The HM is pumped by an off-chip LSU, which is a tunable reference frequency in the range of 19–21 GHz. The frequency of the LSU is chosen such that the difference frequency
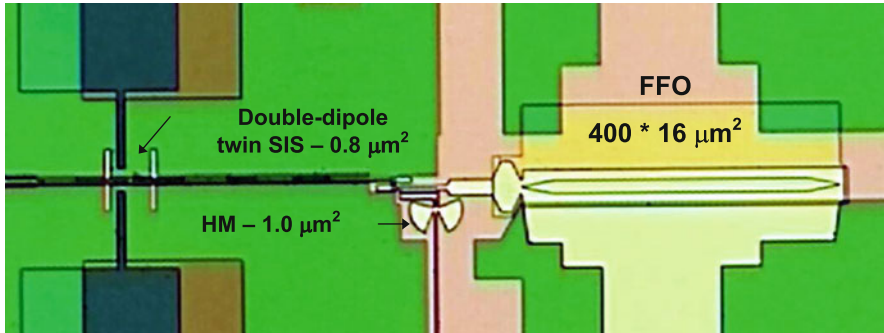
Fig. 10.18 Central part of the SIR chip with double-dipole antenna, twin SIS-mixer, and harmonic mixer for FFO phase-locking

of the nth harmonic of the LSU, generated by the HM, and the FFO is about 4 GHz. This difference signal is then amplified by a cryogenic low-noise HEMT amplifier and down-converted to 400 MHz by using a second reference at 3.6 GHz. Finally, the frequency and phase of this 400 MHz signal is compared against yet another reference frequency of 400 MHz and the resulting error signal is fed back to the FFO. The LSU and the reference signals at 3.6 GHz and at 400 MHz are all phase locked to an internal ultra stable 10 MHz Master Oscillator.

All components of the SIR microcircuits are fabricated in a high quality Nb–AlN/NbN tri-layer on a Si substrate [13]. The receiver chip is placed on the flat back surface of the elliptical silicon lens (forming an integrated lens-antenna) with accuracy 10 μm, determined by the tolerance analysis of the optical system. As the FFO is very sensitive for external electromagnetic interferences, the SIR chip is shielded by two concentric cylinders: the outer cylinder is made of cryoperm and the inner one of copper with a 100 μm coating of superconducting lead. All SIR channel components (including input optical elements) are mounted on a single plate inside a $240 \times 180 \times 80$ mm box cooled by the thermo-straps to the temperature of about 4.2 K.

10.3.3 TELIS-SIR Channel Performance

The TELIS-SIR channel has been characterized in eight micro-windows that have been selected for the flight in (Sweden). These micro-windows have the following LO frequencies:

- 495.04 GHz for $H_2{}^{18}O$
- 496.88 GHz for HDO
- 505.60 GHz for BrO
- 507.27 GHz for ClO
- 515.25 GHz for O_2, pointing, and temperature
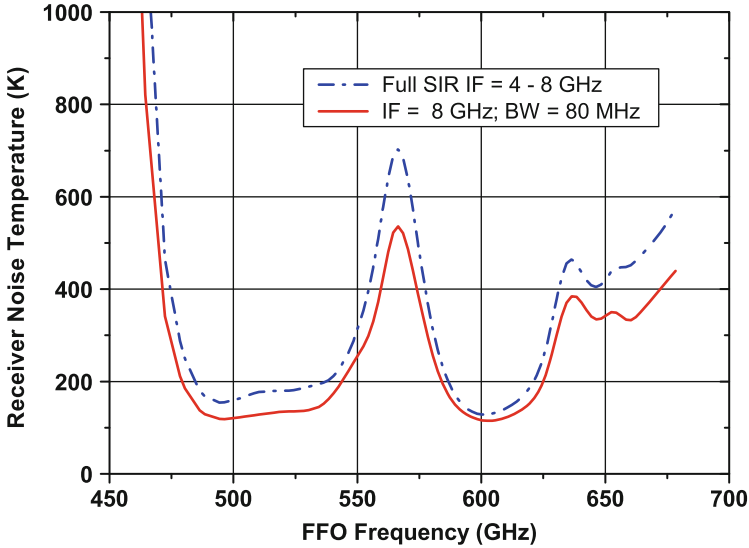
Fig. 10.19 Measured DSB receiver noise temperature of the SIR device selected for flight at 8 GHz IF (*solid line*) and integrated in the 4–8 GHz IF range (*dashed line*)

- 519.25 GHz for BrO and NO_2
- 607.70 GHz for ozone isotopes
- 619.10 GHz for HCl, ClO and HOCl

Initial flight values for the parameters for the FFO, SIS, and HM mixers have been determined for each micro-window. Dedicated algorithms allowing for fast switching between LO frequencies and for in-flight optimization of the SIR have been developed (see below). It takes about 1 min of stabilization and optimization to switch between two LO settings. All experimental results discussed here have been obtained with the SIR flight device.

The measured double sideband (DSB) receiver noise temperature T_R, uncorrected for any loss, is presented in Fig. 10.19 as a function of LO frequency. As can be seen, the noise is well below 200 K at all frequencies of interest, with a minimum of 120 K at 500 and 600 GHz. The noise peak around 540–575 GHz is partially spurious, caused by absorption of water vapor in the path between calibration sources and the cryostat, and partially real – due to properties of the SIS-mixer tuning circuitry. The relatively high noise in this band is of no concern for science observations, since this part of the atmospheric spectrum is obscured by a highly saturated water-vapor line rendering it virtually useless for atmospheric science. The noise as a function of IF is fairly flat in the frequency range 4–8 GHz, as can be seen in Fig. 10.20, where (DSB) receiver noise temperature is plotted as a function of IF. The dependence of the receiver noise temperature on the SIS bias voltage is shown in Fig. 10.21; one can see that for Nb–AlN/NbN circuits there is very wide range of SIS bias voltages where T_R is almost constant.
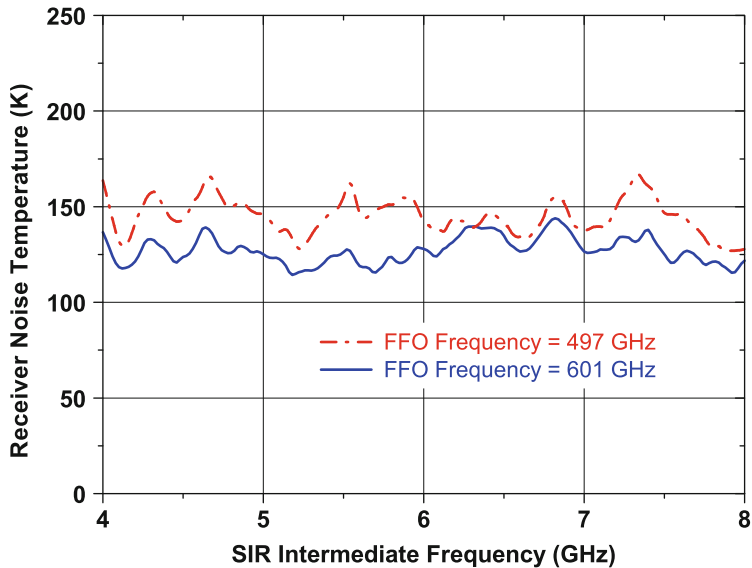
Fig. 10.20 DSB receiver noise temperature as a function of the IF, taken at two FFO frequencies: 497 and 601 GHz
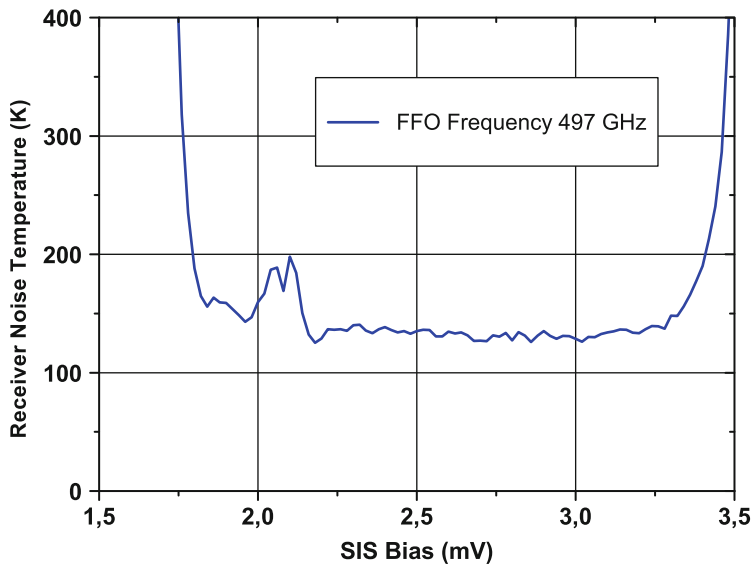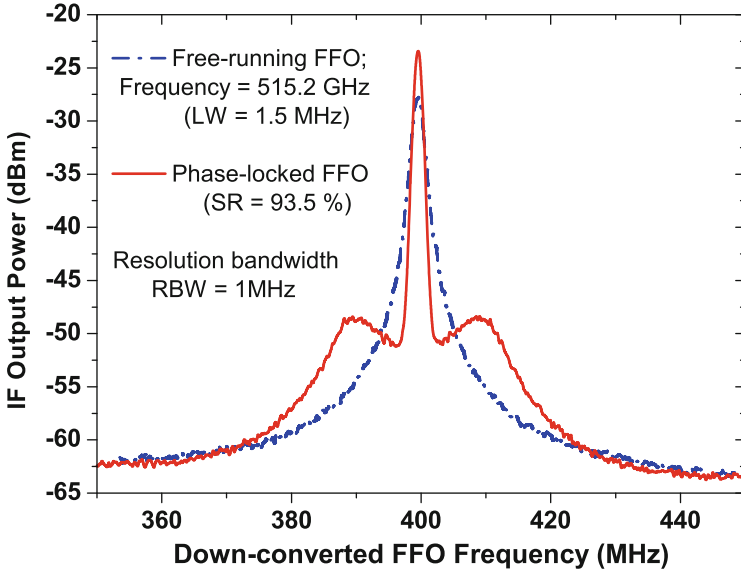

Fig. 10.21 DSB receiver noise temperature as a function of the SIS bias voltage measured at the FFO frequency 497 GHz

Fig. 10.22 Spectra of the FFO operating at 515.2 GHz (*blue dashed line* – frequency locked; *red solid line* – phase-locked). Linewidth (LW) = 1.5 MHz; signal-to-noise ratio (SNR) = 36 dB; spectral ration (SR) = 93.5%. Spectra measured with RBW = 1 MHz, span = 100 MHz

After optimization of the FFO design, the free-running LW between 7 and 0.5 MHz has been measured in the frequency range 350–750 GHz (see Fig. 10.10), which allows to phase lock from 35% to 95% of the emitted FFO. Example of the free-running (frequency-locked) and phase locked spectra of the FFO measured for flight SIR at one of the frequencies selected for first TELIS flight are presented in Fig. 10.22.

Data for five important TELIS frequencies are summarized in Table 10.1. It should be mentioned that the noise of the digital electronics at frequencies of about 1 MHz slightly increases the measured LW value, while the PLL is able to suppress the interference (that results in larger SR than can be expected from measured LW). Note also the dependence of the SR and LW on the FFO bias current related to variation of the differential resistance along FS.

For the TELIS measurement strategy, it is important to know whether the timing of limb sounding should depend on the stability of the complete receiver chain. The stability determines the optimum achievable measurement time for a single integration, and thus the required frequency of the calibration cycle. The stability of the complete TELIS-SIR system has been determined with a noise-fluctuation bandwidth of 17 MHz, and the results [10] are presented in Fig. 10.23. For the two IF channels that are used to determine the Allan variance, it is found that the Allan stability time is about 13.5 s. When the difference of the two channels is taken to determine the Allan variance (this is the so-called spectroscopic, or differential,

Table 10.1 Data for the flight SIR at selected TELIS frequencies

FFO frequency (GHz)	LW (MHz)	SNR (dB)	SR (%)	FFO Ib (mA)
495.04	1.5	32	90	30.7
496.88	1.5	37	93	31.3
515.25	1.5	36	93.5	29.2
607.7	2.1	32	87.7	30
607.7	1.8	32.6	88.6	34
619.1	5.4	25	63.3	30
619.1	4.6	26.8	70.3	34
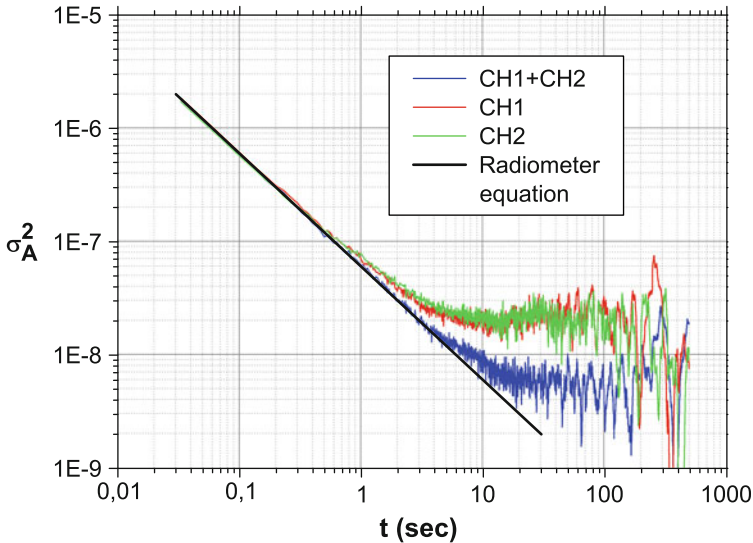
Fig. 10.23 System stability of the SIR channel. FFO is phase locked at 600 GHz. The two lines at the top (*red and green*) represent individual channel variances, the *blue line* is representative of the spectroscopic variance and the *straight black line* corresponds to the radiometer equation

mode), the Allan stability time of 20 s is found. This is comparable to stabilities measured for astronomical receivers.

Within TELIS, a 1.5 s integration time per tangent height is used. This is mainly driven by the required integrated signal levels at the autocorrelator input. The stability of the SIR channel therefore poses no constraints on the observing strategy.

The SIR is a complicated device as it contains multiple interactive superconducting elements: an SIS mixer, an FFO, and an HM for the FFO phase locking. Special algorithms and procedures have been developed and tested to facilitate characterization of the SIR at reasonable timescales and for the SIR control during the flight. These routines include:

- Fast definition of the FFO operational conditions (both on the FS and in the flux-flow regimes).
- Measurements of the free-running FFO LW.

- Optimization of the LSU and HM parameters.
- Optimization of the PLL operation.
- Minimization of the SIR noise temperature.
- Setting all predefined SIR parameters in the exact sequence for control during the flight.
- Continuous monitoring of the main SIR parameters.
- Adjustment (or recovering) of the SIR operational state.

10.3.4 Kiruna Campaigns and Preliminary Science Results

TELIS had two successful scientific campaigns from Kiruna, North-Sweden, in March 2009 and in January 2010. The instrument was launched together with the MIPAS instrument on the MIPAS-B2 gondola (see Fig. 10.24). The launch of both flights took place around midnight. During the ascents, the SIR channel behaved nominally and already after 30 min the first spectra were recorded. In the 2009 flight, the first flight ceiling of 35 km was reached after 3 h and 1 h later the flight continued at 28 km altitude. In the 2010 flight, the ascent took more than 4 h to reach a flight ceiling of 34 km where the balloon stayed for the remainder of the flight. Several night recordings were taken, necessary for background measurements for species with a diurnal cycle and for instrument calibration. The instrument proved to be stable against the strong temperature variations of the atmosphere during ascent (with ambient temperatures as low as $-90\,°C$) and during sunrise. The south eastern wind allowed for long flights of about 12 h over Finland during both


Fig. 10.24 TELIS-MIPAS launch at Esrange, Sweden; March 2009. Balloon size: $400,000\,m^3$; payload weight: 1,200 kg

campaigns. After sunrise, the diurnal cycle of various species was monitored and in total several hundred limb sequences have been recorded in each flight. The MIPAS-TELIS balloon system performed nominally during the flight and after the parachute landing and recovery, the instruments were found to be undamaged, allowing for post-flight checks and calibration measurements.

The science goals of the campaign from Kiruna, North Sweden, were threefold: investigation of the stratospheric hydrological cycle by measurements of isotopic water, catalytic ozone destruction by chlorine chemistry, and the bromine content of the stratosphere. In addition, measurements were performed for space-borne instruments (ENVISAT satellite and in 2010 also SMILES aboard the International Space Station). Data presented in Fig. 10.25 prove the capabilities of the TELIS-SIR channel for high-resolution spectroscopy. In this case, the FFO frequency is tuned to 505.600 GHz, the telescope is 6 degrees up-looking, and the gondola altitude is 35.780 km. The width of the ozone lines are almost fully determined by atmospheric conditions (Doppler and pressure broadening) and are about 10 MHz, as expected.

Chlorine ozone destruction peaks in the arctic winter and/or spring when the so-called polar vortex breaks up. During this event, the ClO radical, responsible for catalytic ozone destruction, becomes available in huge amounts. However, chlorine is also stored in nonreactive reservoir species of which HCl is an important member. The amount of HCl in the stratosphere is a measure of the total nonactive Cl content and is as such an important species to monitor in ozone chemistry studies.

In Fig. 10.26 measured spectra are shown in which the HCl line at IF $= 6.81$ GHz is well pronounced for line of sights. A line of sight is determined by the flight
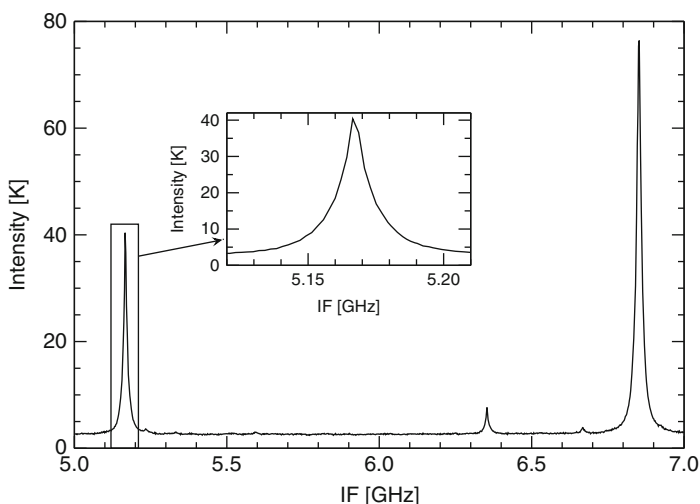
Fig. 10.25 Ozone spectrum recorded during the 2009 campaign with the SIR channel (FFO frequency $= 505.6$ GHz) from an altitude of 35.780 km and with the telescope pointing 6° upward. The width of the lines is ca. 10 MHz and is fully determined by atmospheric conditions. The intensity of the received signal in Kelvin is plotted as ordinate of the graphs
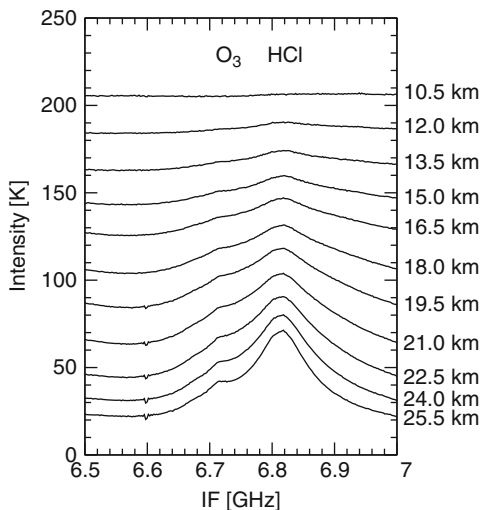
altitude of the balloon platform and the tilt of the telescope. Each line of sight results in different altitude sensitivities and effectively probes different parts of the atmosphere. The altitudes mentioned in Fig. 10.26 refer to the lowest probed altitude, the tangent height, for a certain line of sight and generally corresponds to the altitude for which the measurement is mostly sensitive.

Bromine depletes ozone even more aggressively than chlorine on a per molecule basis, but its abundances are much lower. In fact, the total amount of stratospheric bromine is still not settled and is currently one of the main uncertainties in the importance of bromine in ozone depletion.

In 2009, the flight took place in nonvortex conditions whereas in 2010 the flight was in the polar vortex. The diurnal cycle of ClO has been observed in both flights, albeit with a much higher time resolution in the 2010 flight (ca. 1 min). In 2009, BrO has been detected, although barely as the line was superimposed on another spectral feature. However, in 2010 the BrO line, with a level of only ca. 0.3 K, was isolated and clearly detected. The data reduction is on-going but the first spectra for HCl, ClO, and BrO are presented in Figs. 10.26, 10.27, and 10.28, respectively.

10.3.5   SIR for Noninvasive Medical Diagnostics

High sensitivity and spectral resolution of the integrated spectrometer enables the analysis of multicomponent gas mixtures. Exhaled air of human includes about 400 gases, of which some can be indicators of various diseases and pathology. For example, nitric oxide, NO, was detected in the exhaled air of patients suffering from bronchial asthma, pneumonia, and other chronic inflammatory diseases of upper airways. Besides, nitric oxide may have an effect on the reaction of tumors and

Fig. 10.27 ClO spectra recorded during the 2010 campaign with the SIR channel (FFO frequency = 507.3 GHz) from an altitude of ca. 34 km. The two sets of spectra correspond, respectively, to 25 and 19 km tangent heights, i.e. the altitudes for which these spectra are most sensitive. The increase of ClO over time is clearly visible. The intensity of the received signal in Kelvin is plotted as ordinate of the graphs
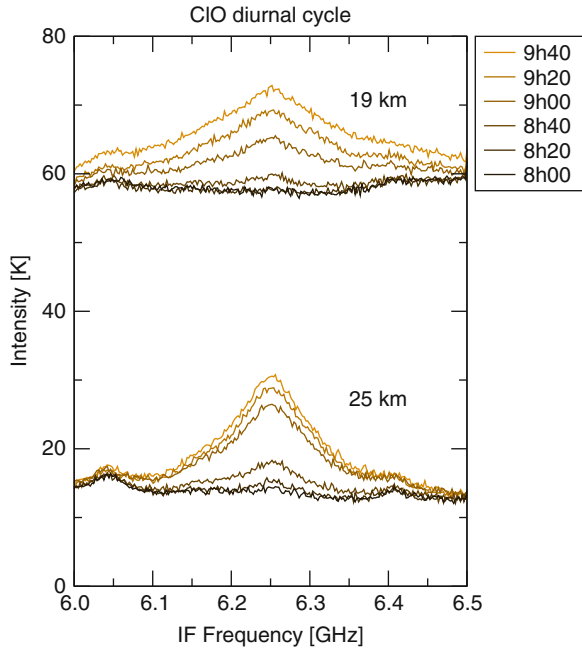
Fig. 10.28 BrO spectra recorded during the 2010 campaign with the SIR channel (FFO frequency = 519.3 GHz) from an altitude of ca. 34 km. In the daytime measurement (*orange*), the BrO line is visible at 5.6 GHz. During the nighttime measurement (*black*), BrO is absent, as expected. The shown tangent heights are from top to bottom 26, 28, 30, and 32 km, i.e. the altitudes for which these spectra are most sensitive. The intensity of the received signal in Kelvin is plotted as ordinate of the graphs
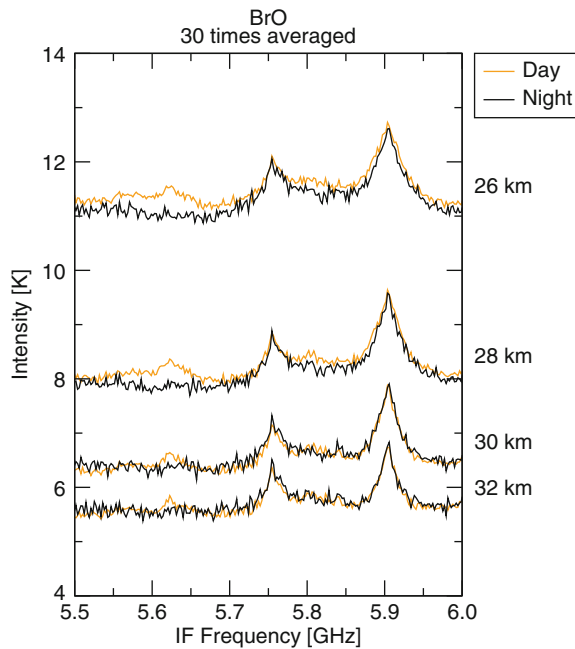
healthy tissues on radiation therapy. Another example may concern the opportunity of noninvasive diagnostics of gastritis or peptic ulcer of the stomach by measuring the concentration of ammonia in exhaled air. Nowadays urease respiratory tests (application of urea with C^{13}) are mainly used to detect the diseases. However, the method is quite expensive and its sensitivity is restricted by natural variations of C^{13} in exhaled air during the procedure. Natural concentrations of ammonia instead are quite low, so the measurement of the ammonia concentration could be a good alternative. Another important application concerns the noninvasive diagnostics of diabetes, where exhaled acetone is an indicator.

A laboratory setup for spectral analysis of the exhalted air has been developed at IREE (input frequency range 480–630 GHz, noise temperature below 200 K over the range, spectral resolution below 1 MHz), based on the integrated spectrometer for atmosphere monitoring. The instrument parameters allow us to measure the spectral lines of the rotational transitions for most of the substances in the exhaled air. The laboratory setup has been developed and demonstrated using the gases OCS and NH_3 in the laboratory gas cell. Clear and well-defined response has been measured at the expected frequencies of spectral lines for pressures down to 10^{-3} mBar. Examples of the NH_3 spectra recorded by the SIR with the Fast Fourier Transform Spectrometer (FFTS) as a back-end, and by the novel technique based on application of the additional oscillator are presented in Fig. 10.29 and 10.30, respectively. The possibility to measure the spectral response in a few seconds has been demonstrated experimentally. This allows to carry on the real-time medical survey. First spectral measurements by the integrated receiver of exhalted air in the sub-THz range have demonstrated good selectivity and speed of the analysis as well as high sensitivity.
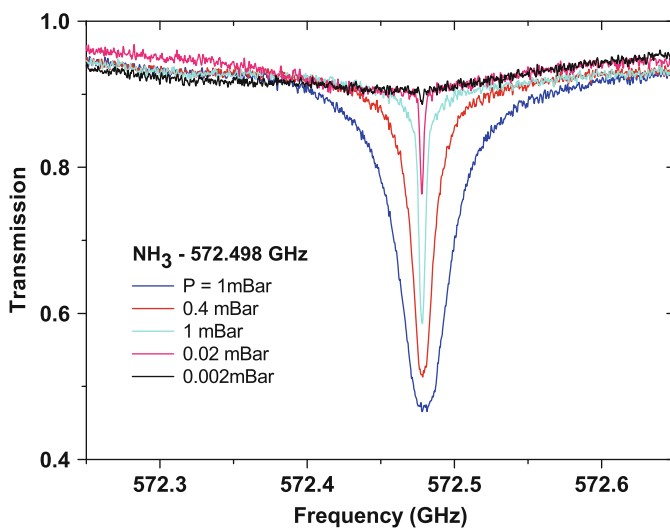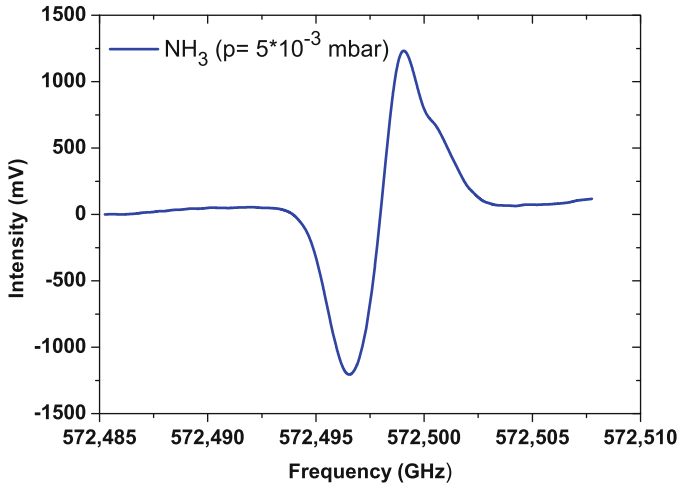

Fig. 10.29 NH_3 spectra measured by the SIR with FFTS back-end at different pressures

Fig. 10.30 Response (derivative of the spectral line), measured for NH_3 gas by the integrated receiver with implementation of novel technique (details will be published elsewhere)

For example, we have measured ammonia concentration with sensitivity on the order of 10^{-9} (1 ppb).

10.4 Summary

The capability of the SIR for highresolution atmospheric spectroscopy has been successfully proven with scientific balloon flights from Kiruna, North Sweden. During the two 12-h missions, phase locked SIR operation and frequency switching in the 480–650 GHz frequency range has been realized. An intrinsic spectral resolution of the SIR well below 1 MHz has been confirmed by CW signal measurements in the laboratory. An uncorrected DSB noise temperature below 120 K has been measured for the SIR when operated with a phase locked FFO at an IF bandwidth of 4–8 GHz. To ensure remote operation of the phase locked SIR several software procedures for automatic control have been developed and tested. The first tentative HCl profile has been presented and its quality looks promising for future data reduction. Diurnal cycles of ClO and BrO have been observed at different viewing configurations (altitude), with BrO line level of only about 0.5 K. Possibilities to use the SIR devices for analysis of the breathed out air at medical survey have been demonstrated. The SIR can be considered as an operational device, ready for many applications.

References

1. V.P. Koshelets, S.V. Shitov, L.V. Filippenko, A.M. Baryshev, H. Golstein, T. de Graauw, W. Luinge, H. Schaeffer, H. van de Stadt First implementation of a superconducting integrated receiver at 450 GHz. Appl. Phys. Lett. **68**(9), 1273 (1996)
2. V.P. Koshelets, S.V. Shitov, Integrated superconducting receivers. Supercond. Sci. Technol. **13**, R53 (2000)
3. P. Yagoubov, R. Hoogeveen, M. Torgashin, A. Khudchenko, V. Koshelets, N. Suttiwong, G. Wagner, M. Birk, 550–650 GHz spectrometer development for TELIS. Proc. ISSTT 338 (2006)
4. V.P. Koshelets, A.B. Ermakov, L.V. Filippenko, A.V. Khudchenko, O.S. Kiselev, A.S. Sobolev, M.Y.u. Torgashin, P.A. Yagoubov, R.W.M. Hoogeveen, W. Wild Iintegrated submillimeter receiver for TELIS. IEEE Trans. Appl. Supercond. **17**, 336 (2007)
5. G. de Lange, D. Boersma, J. Dercksen, P. Dmitriev, A. Ermakov, L. Filippenko, H. Golstein, R. Hoogeveen, L. de Jong, A. Khudchenko, N. Kinev, O. Kiselev, B. van Kuik, A. de Lange, J. van Rantwijk, A. Sobolev, M. Torgashin, E. de Vries, P. Yagoubov, V. Koshelets, Development and characterization of the superconducting integrated receiver channel of the TELIS atmospheric sounder. Supercond. Sci. Technol. **23**(4), 045016 (2010)
6. T. Nagatsuma, K. Enpuku, F. Irie, K. Yoshida, Flux-flow type Josephson oscillator for millimeter and submillimeter wave region. J. Appl. Phys. **54**, 3302, (1983), see also Pt. II: J. Appl. Phys. **56**, 3284 (1984); Pt. III, J. Appl. Phys. **58**, 441 (1985); Pt. IV, J. Appl. Phys. **63**, 1130 (1988)
7. V.P. Koshelets, P.N. Dmitriev, A.B. Ermakov, A.S. Sobolev, M.Y.u. Torgashin, V.V. Kurin, A.L. Pankratov, J. Mygind, Optimization of the phase-locked flux-flow oscillator for the submm integrated receiver. IEEE Trans. Appl. Supercond. **15**, 964–967 (2005)
8. I. Mehdi, THz local oscillator technology. Proc. SPIE **5498**, 103 (2004)
9. R.W.M. Hoogeveen, P.A. Yagoubov, A. de Lange, A.M. Selig, V.P. Koshelets, B.N. Ellison, M. Birk, Proc. SPIE **5978**, 440 (2005)
10. R.W.M. Hoogeveen, P.A. Yagoubov, G. de Lange, A. de Lange, V. Koshelets, M. Birk, B. Ellison, Proc. SPIE **6744**, 67441U-1 (2007)
11. F. Friedl-Vallon, G. Maucher, M. Seefeldner, O. Trieschmann, A. Kleinert, A. Lengel, C. Keim, H. Oelhaf, H. Fischer, Appl. Opt. **43**, 3335 (2004)
12. V.P. Koshelets, S.V. Shitov, A.B. Ermakov, O.V. Koryukin, L.V. Filippenko, A.V. Khudchenko, M.Y.u. Torgashin, P. Yagoubov, R. Hoogeveen, O.M. Pylypenko, Superconducting integrated receiver for TELIS. IEEE Trans. Appl. Supercond. **15**, 960–963, 2005
13. V.P. Koshelets, S.V. Shitov, A.V. Shchukin, L.V. Filippenko, J. Mygind, A.V. Ustinov, Self-pumping effects and radiation linewidth of Josephson flux flow oscillators. Phys Rev B **56**, 5572–5577 (1997)
14. P.N. Dmitriev, I.L. Lapitskaya, L.V. Filippenko, A.B. Ermakov, S.V. Shitov, G.V. Prokopenko, S.A. Kovtonyuk, V.P. Koshelets, High quality Nb-based integrated circuits for high frequency and digital applications. IEEE Trans. Appl. Supercond. **13**(2), 107–110 (2003)
15. M.Y.u. Torgashin, V.P. Koshelets, P.N. Dmitriev, A.B. Ermakov, L.V. Filippenko, P.A. Yagoubov, Superconducting integrated receivers based on Nb-AlN-NbN circuits. IEEE Trans. Appl. Supercond. **17**, 379–382 (2007)
16. V.P. Koshelets, S.V. Shitov, A.V. Shchukin, L.V. Filippenko, J. Mygind, Linewidth of submillimeter wave flux-flow oscillators. Appl. Phys. Lett. **69**, 699–701 (1996)

17. V.P. Koshelets, J. Mygind, Flux flow oscillators for superconducting integrated submm wave receivers, in Studies of High Temperature Superconductors, **39**, ed. by A.V. Narlikar (NOVA Science Publishers, New York, 2001) 213–244

18. V.P. Koshelets, A.B. Ermakov, P.N. Dmitriev, A.S. Sobolev, A.M. Baryshev, P.R. Wesselius, J. Mygind, Radiation linewidth of flux flow oscillators. Supercond. Sci. Technol. **14**, 1040–1043 (2001)

19. V.P. Koshelets, S.V. Shitov, P.N. Dmitriev, A.B. Ermakov, L.V. Filippenko, V.V. Khodos, V.L. Vaks, A.M. Baryshev, P.R. Wesselius, J. Mygind, Towards a phase-locked super-conducting integrated receiver: prospects and limitations. Phys. C **367**, 249–255 (2002)

20. A.L. Pankratov, Form and width of spectral line of a Josephson flux flow oscillator. Phys. Rev. B. **65**, 054504 (2002)

21. V.P. Koshelets, A.B. Ermakov, S.V. Shitov, P.N. Dmitriev, L.V. Filippenko, A.M. Baryshev, W. Luinge, J. Mygind, V.L. Vaks, D.G. Pavel'ev, Superfine resonant structure on IVC of long Josephson junctions and its influence on flux flow oscillator linewidth. IEEE Trans. Appl. Supercond. **11**, 1211–1214 (2001)

22. P. Berberich, R. Buemann, H. Kinder, Monochromatic phonon generation by the Josephson effect. Phys. Rev. Lett. **49**(20), 1500–1503 (1982)

23. V.P. Koshelets, S.V. Shitov, L.V. Filippenko, P.N. Dmitriev, A.B. Ermakov, A.S. Sobolev, M.Y.u. Torgashin, A.L. Pankratov, V.V. Kurin, P. Yagoubov, R. Hoogeveen Superconducting phase-locked local oscillator for a submm integrated receiver. Supercond. Sci. Technol. **17**, \$127–\$131 (2004)

24. A.L. Pankratov, V.L. Vaks, V.P. Koshelets, Spectral properties of phase locked flux flow oscillator. J. Appl. Phys. **102**, 0629 (2007)

25. A.V. Khudchenko, V.P. Koshelets, P.N. Dmitriev, A.B. Ermakov, P.A. Yagoubov, O.M. Pylypenko, Cryogenic phase detector for superconducting integrated receiver. IEEE Trans. Appl. Supercond. **17**, 606–608 (2007)

26. E. Schomburg, R. Scheuerer, S. Brandl, K.F. Renk, D.G. Paveliev, Y.u. Koschurinov, V. Ustinov, A. Zhukov, A. Kovsh, P.S. Kopev, Electron. Lett. **35**(17) (1999)

27. http://www2.rohde-schwarz.com/product/smf100a.html

28. P. Yagoubov, H. van de Stadt, R. Hoogeveen, V. Koshelets, M. Birk, A. Murk, in *Proceedings of the 28th ESA Antenna Workshop on Space Antenna Systems and Technologies*, Noordwijk, 2, 763 (2005)

29. P.A. Yagoubov, W.J. Vreeling, H. van de Stadt, R.W.M. Hoogeveen, O.V. Koryukin, V.P. Koshelets, O.M. Pylypenko, A. Murk, in *Proceedings of the 16th Intern. Conf. on Space Terahertz Technology, Gothenburg*, 438 (2005)

30. A. Murk, P. Yagoubov, U. Mair, M. Birk, G. Wagner, H. van de Stadt, R. Hoogeveen, N. Kämpfer, *Proc. of the 28th ESA Antenna Workshop on Space Antenna Systems and Technologies, Noordwijk*, 757 (2005)

31. B.N. Ellison, B.P. Moyna, D.N. Matheson, A. Jones, S.M.X. Claude, C. Mann, B.J. Kerridge, R. Siddans, R. Munro, W.J. Reburn, in *Proceedings of 2nd ESA Workshop on Millimetre Wave Technology and Applications, Espoo*, (1998)

32. S. Cherednichenko, V. Drakinskiy, T. Berg, P. Khosropanah, E. Kollberg, Rev. Sci. Instrum. **79**, 034501 (2008)

33. A. Emrich, S. Andersson, M. Knis *Proceedings of the joint 31st International Conference on Infrared Millimeter Waves and 14th International Conference on Teraherz Electronics, Shanghai*, 314 (2006)